

# Airborne Pseudolite Distributed Positioning based on Real-time GNSS PPP

Panpan Huang, Chris Rizos and Craig Roberts

*(School of Civil and Environmental Engineering,  
University of New South Wales, Australia)*  
(E-mail: [p.huang@student.unsw.edu.au](mailto:p.huang@student.unsw.edu.au))

Airborne-Pseudolite (A-PL) systems have been proposed to augment Global Navigation Satellite Systems (GNSSs) in difficult areas where GNSS-only navigation cannot be guaranteed due to signal blockages, signal jamming, etc. One of the challenges in realising such a system is to determine the coordinates of the A-PLs to a high accuracy. The GNSS Precise Point Positioning (PPP) technique is a possible alternative to differential GNSS techniques such as those that generate Real-Time Kinematic (RTK) solutions. To enhance the A-PL positioning performance in GNSS challenged areas, it is assumed that inter-PL range measurements are also used in addition to GNSS measurements. When processing these new measurements, cross-correlations among A-PL estimated states introduced during measurement updates need to be accounted for so as to obtain consistent estimated states. In this paper, a distributed algorithm based on a Split Covariance Intersection Filter (SCIF) is proposed. Three commonly used means of implementing the SCIF algorithm are analysed. Another challenge is that real-time GNSS PPP relies on the use of precise satellite orbit and clock information. One problem is that these real-time orbit and satellite clock error corrections may not be always available, especially for moving A-PLs in challenging environments when signal outages occur. To maintain A-PL positioning accuracy using GNSS PPP, it is necessary to predict these error corrections during outages. Different prediction models for orbit and clock error corrections are discussed. A test was conducted to evaluate the A-PL positioning based on GNSS PPP and inter-PL ranges, as well as the performance of error prediction modelling. It was found that GNSS PPP combined with inter-PL ranges could achieve better converged positioning accuracy and a reduction in convergence time of GNSS PPP. However, the performance of GNSS PPP with inter-PL ranges was degraded by observing A-PLs with limited positioning accuracy. Although the performance improvement achieved by the SCIF-based distributed algorithms was smaller than that by the centralised algorithm, greater robustness in dealing with deteriorated observed A-PLs' trajectory data was demonstrated by the distributed algorithms. In addition, short-term prediction models were analysed, and their performance was shown to reduce the effect of error correction outages on A-PL positioning accuracy.

## KEY WORDS

1. PPP.
2. A-PL positioning.
3. SCIF.
4. Orbit and clock corrections.

Submitted: 15 July 2018. Accepted: 16 March 2019. First published online: 22 April 2019.

1. INTRODUCTION. Pseudolite, or “pseudo-satellite” (PL) systems are intended to provide suitably equipped users with position, velocity or timing information, based on measurements made on Global Navigation Satellite System (GNSS)-like signals transmitted by the PLs. By either augmenting GNSS with extra GNSS-like signals, or operating independently of GNSS with sufficient PL signals, such systems have been proposed in order to address Position, Navigation and Timing (PNT) requirements for a number of application areas, such as underground or indoor positioning, construction machine and port automation, deformation monitoring, operations in deep open-cut mines and wherever GNSS-derived PNT is not available due to poor satellite visibility and/or bad signal reception conditions (Kim et al., 2008). There are two basic types of PL systems: terrestrial PL (T-PL) systems and airborne PL (A-PL) systems.

With PLs mounted on aircraft, balloons, airships or unmanned aerial vehicles (UAVs) A-PL systems have better vertical observability and suffer less significant multipath effects as well as fewer “near-far” problems compared with T-PL systems (Chandu et al., 2011; Lee et al., 2016). The A-PLs are generally configured to be either station-keeping (that is, hovering or keeping a near-stationary position in the sky) or flying around the service area (for example, following some pre-defined trajectory) (Garcia-Crespillo et al., 2015; He et al., 2016; Lee et al., 2017). To realise such an A-PL system, one of the challenges is to precisely determine the positions of the A-PLs on a continuous basis. A number of positioning methods based on GNSS have been proposed. For example, based on the “Inverted GNSS” (IGNSS) principle, the A-PLs could be monitored by a network of ground stations (Tsujii et al., 2001). To accurately position the A-PL in a real-time continuous mode, the Real-Time Kinematic (RTK) technique with one or more reference stations would be typically used (Lee et al., 2016). As an alternative approach, real-time Precise Point Positioning (PPP) has also been proposed for continuous positioning (Gross et al., 2016). This method does not have stringent requirements for simultaneous measurements made by the A-PLs and ground-based reference stations, or limitations on maintaining a comparatively short baseline to ground reference stations (typically of the order of several tens of kilometres). Furthermore, the PPP method is able to deliver comparable positioning accuracy, with lower computational burden and better long-term repeatability than RTK-based methods (Bisnath and Gao, 2009). However, there are some problems in using real-time GNSS PPP when there is GNSS signal degradation or blockage, such as longer convergence time, loss of precise orbit and clock correction data, etc. To reduce the convergence time, a number of methods have been proposed, augmenting GNSS PPP with additional information. For example, commonly used GNSS PPP augmentations add more observations, using multiple frequency and/or GNSS constellations, including BeiDou (BDS), Galileo, modernised Global Positioning System (GPS) and Globalnaya Navigazionnaya Sputnikovaya Sistema (GLONASS) (Tegeedor et al., 2014), or tightly integrating with an Inertial Navigation System (INS) (Gao et al., 2017; Liu et al., 2016). Another strategy is to enable integer ambiguity resolution with precise (externally provided) atmospheric corrections to realise rapid convergence (de Oliveira et al., 2017; Geng et al., 2010; Teunissen and Khodabandeh, 2015).

In this paper, the real-time GNSS PPP method is proposed for A-PL positioning. To enhance PPP performance for the A-PL in GNSS challenged areas, inter-PL range measurements could be combined with GNSS measurements. To process such relative measurements, cross correlations among the A-PL estimated states introduced during the measurement updates have to be accounted for in order to obtain consistent estimated

states. There are two commonly used strategies to address this problem: centralised and decentralised approaches. The centralised algorithm is implemented with a master A-PL or a Fusion Centre (FC) or central processor, gathering and processing information from all A-PLs in the network at every time instant (Howard et al., 2002). Then the FC broadcasts back the estimated positions to each A-PL. This approach suffers from high computational and communication costs. Moreover, it is susceptible to a single point of failure. To avoid communicating with a master A-PL or FC, and reducing the communication bandwidth, decentralised algorithms have been developed. The decentralised algorithms can also be divided into two categories (Kia et al., 2016). One is the tightly-coupled class of algorithms, often referred to as the centralised-equivalent approach, which has the computational load of the centralised algorithm distributed among the entire network and accurately tracks the cross correlations. However, such algorithms still suffer from relatively high computational, communication and/or data storage costs, as a synchronous communication network for information exchange is required (Kia et al., 2016). The other category is the loosely-coupled class of algorithms. Although the exact cross correlations are not maintained for this type of decentralised algorithm, the drawbacks in the tightly-coupled decentralised algorithms can be addressed. To obtain estimation consistency, Covariance Intersection Filter (CIF) and Split CIF (SCIF) algorithms can be used (Li and Nashashibi, 2013; Wanasinghe et al., 2014; Wu et al., 2017). The SCIF algorithm is able to maintain the known independent information in the estimates, which is treated as correlated with all estimates among the network by the CIF. Therefore, the decentralised algorithm based on the SCIF is more suitable to use for the A-PL distributed positioning in this paper, as only the states involved in the inter-PL ranges are known to be correlated with each other.

Real-time GNSS PPP depends on receiving Real-Time Service (RTS) products such as precise orbit and satellite clock corrections transmitted continuously using, for example, the Network Transport of Radio Technical Commission for Maritime Services (RTCM) by Internet Protocol (NTRIP). Unfortunately, the availability of these real-time corrections is often not 100% (Hadas and Bosy, 2015). It can be worse for moving A-PLs in challenging environments where an outage of a caster connection is often likely to occur. To maintain the A-PL positioning accuracy based on GNSS PPP during periods of interruption, the real-time orbit and clock corrections can be predicted using appropriate models. The orbit prediction models are generally based on polynomial models with different orders (Hadas and Bosy, 2015; El-Mowafy et al., 2017). It has been demonstrated that this type of fitting model is able to predict short-term International GNSS Service (IGS) RTS orbit corrections with better than 10 cm accuracy. For long-term orbit predictions it has been proposed to use IGS Ultra-rapid (IGU) orbit corrections as a substitute for RTS orbit corrections, as these two IGS products are numerically compatible with each other (El-Mowafy, 2017). Unlike the orbit corrections characterising a polynomial pattern, the satellite clock corrections have more complex characteristics, including both periodic and stochastic variations (Heo et al., 2010; Huang et al., 2014). The clock prediction models generally consist of two parts. One part represents linear or nonlinear coupling characteristics of the clock corrections using a polynomial model. The other part is often in sinusoidal form and describes the periodic variation behaviour of the clock. These models can be used for long-term clock predictions over a few hours and even for a day. However, these models need long-term fitting data. In this paper only short-term predictions of orbit and satellite clock corrections are studied with fitting data less than 15 min, as this can be implemented online with A-PL positioning without storing the long-term fitting data.

The remainder of this paper is organised as follows. In Section 2, the SCIF algorithm is first reviewed and then the A-PL positioning method based on GNSS PPP combined with inter-PL ranges using the SCIF algorithm is described. In Section 3, the short-term predictions of orbit and satellite clock corrections using different models are introduced. To evaluate the A-PL positioning performance, the results of a semi-simulation are analysed in Section 4. Finally, some concluding remarks are presented.

**2. A-PL DISTRIBUTED POSITIONING.** All the A-PLs in the proposed A-PL system are assumed to be time-synchronised. The time synchronisation can be realised by chronologically synchronising the positioning signals of all the A-PLs to the time base of a designated reference transmitter with a kinematic Time Lock Loop (TTL) (Small, 2017). The reference transmitter can be synchronised to an A-PL or a GPS satellite. The kinematic TTL is implemented by repeatedly adjusting frequency and time differences between the A-PL of interest and the reference transmitter with the self-monitored trajectory data, including location, velocity and acceleration. The time synchronisation among all the A-PLs can also be realised using the Two-Way Time and Frequency Transfer (TWTFT) method by calculating the clock difference of ranging differential delay and error compensating between the A-PL of interest and one master A-PL as the reference without the need for A-PL accurate positions (He et al., 2016). In this paper, the A-PL system is assumed to be able to maintain time synchronisation during the entire mission. Each A-PL can be positioned using a GNSS receiver for receiving and processing signals from satellites, and a PL receiver for receiving and processing signals from other PLs.

**2.1. SCIF algorithm.** Consider a pair of state estimates  $\{\hat{\mathbf{x}}_i, \mathbf{P}_i\}$ , where  $i = \{1, 2\}$ , and  $\hat{\mathbf{x}}_i$  and  $\mathbf{P}_i$  represent the estimated state vector and the corresponding error covariance matrix, respectively. If the two estimates are independent from one another, the fused state and its corresponding error covariance can be derived from the general Kalman filter relations (Julier and Uhlmann, 1997):

$$\begin{aligned} \mathbf{P} &= (\mathbf{P}_1^{-1} + \mathbf{P}_2^{-1})^{-1} \\ \hat{\mathbf{x}} &= \mathbf{P} (\mathbf{P}_1^{-1} \hat{\mathbf{x}}_1 + \mathbf{P}_2^{-1} \hat{\mathbf{x}}_2) \end{aligned} \quad (1)$$

When there is correlation between these two estimates, the fused results in Equation (1) would be inconsistent and would have optimistic measures of their quality (Carrillo-Arce et al., 2013). To deal with the correlation between two estimates, CIF can be used (Julier and Uhlmann, 1997). CIF uses a convex combination of the means and covariances of the two estimates, which theoretically yields a consistent estimate for any degree of correlation between two input estimates:

$$\begin{aligned} \mathbf{P}^{-1} &= \omega \mathbf{P}_1^{-1} + (1 - \omega) \mathbf{P}_2^{-1} \\ \hat{\mathbf{x}} &= \mathbf{P} [\omega \mathbf{P}_1^{-1} \hat{\mathbf{x}}_1 + (1 - \omega) \mathbf{P}_2^{-1} \hat{\mathbf{x}}_2] \end{aligned} \quad (2)$$

where  $\omega \in [0, 1]$  is a scalar parameter, which can be optimised with respect to different criteria, such as minimising the trace or the determinant of  $\mathbf{P}$ .

Consider two PLs,  $\text{PL}_i$  and  $\text{PL}_j$ , in a network of  $N$  PLs with states at time instant  $k$  denoted as  $\mathbf{x}_k^i$  and  $\mathbf{x}_k^j$ , and their corresponding covariance  $\mathbf{P}_k^i$  and  $\mathbf{P}_k^j$ , respectively. The

relative measurement between the two PLs can be expressed as (Carrillo-Arce et al., 2013):

$$\mathbf{z}_k^{ij} = \mathbf{H}_k^{ij} \left( \mathbf{x}_k^i - \mathbf{x}_k^j \right) + \mathbf{n}_k^{ij} \tag{3}$$

where  $\mathbf{z}_k^{ij}$  denotes the measurement,  $\mathbf{H}_k^{ij}$  is an orthogonal matrix which enables the state of either PL to be expressed in terms of the other PL state and  $\mathbf{n}_k^{ij}$  is the zero-mean white Gaussian measurement noise with covariance  $\mathbf{R}_k^{ij}$ . PL<sub>i</sub> is assumed to be the one of interest and has the prediction state  $\hat{\mathbf{x}}_{k|k-1}^i$  and corresponding covariance  $\mathbf{P}_{k|k-1}^i$  derived using standard Kalman Filter (KF) methods such as the Extended Kalman Filter (EKF). When the relative measurement from PL<sub>j</sub> is received by PL<sub>i</sub> the information on state  $\hat{\mathbf{x}}_{k|k-1}^j$  and covariance  $\mathbf{P}_{k|k-1}^j$  of PL<sub>j</sub> is also shared with PL<sub>i</sub>. With the received relative information, PL<sub>i</sub> can directly generate an estimate and corresponding covariance from the relative measurement:

$$\begin{cases} \hat{\mathbf{x}}_k^{i*} = \hat{\mathbf{x}}_{k|k-1}^j + \left( \mathbf{H}_k^{ij} \right)^T \mathbf{z}_k^{ij} \\ \mathbf{P}_k^{i*} = \mathbf{P}_{k|k-1}^j + \mathbf{H}_k^{ij} \mathbf{R}_k^{ij} \left( \mathbf{H}_k^{ij} \right)^T \end{cases} \tag{4}$$

At this instant two pairs of state and corresponding covariance of PL<sub>i</sub>, one from the time update and one from the relative measurement update, are derived. The fusion of these two pairs of estimates can then be performed using Equation (2). However, the relative measurement cannot always be expressed as in Equation (3) with an orthogonal matrix  $\mathbf{H}_k^{ij}$ , which is often in a nonlinear form. When  $\mathbf{H}_k^{ij}$  is in any other form it is not possible to directly calculate  $\hat{\mathbf{x}}_k^{i*}$  in Equation (4). To use the relative measurement to update the propagated state and covariance, a transformation of the relative measurements needs to be implemented.  $\mathbf{x}_{k,m}^i = \mathbf{H}_k^{ij} \mathbf{x}_k^j + \mathbf{n}_k^{ij}$  can be derived from Equation (3) using the transformation (Li and Nashashibi, 2013):

$$\mathbf{x}_{k,m}^i = \mathbf{H}_k^{ij} \hat{\mathbf{x}}_{k|k-1}^j + \mathbf{z}_k^{ij} \tag{5}$$

The covariance corresponding to  $\mathbf{x}_{k,m}^i$  is given by  $\mathbf{P}_{k,m}^i = \mathbf{H}_k^{ij} \mathbf{P}_{k|k-1}^j \left( \mathbf{H}_k^{ij} \right)^T + \mathbf{R}_k^{ij}$ . The fusion can be performed after the relative measurement update in KF methods as follows:

$$\begin{aligned} \mathbf{K}_k^* &= \mathbf{P}_{k|k-1}^i \left( \mathbf{H}_k^{ij} \right)^T \left[ \mathbf{H}_k^{ij} \mathbf{P}_{k|k-1}^j \left( \mathbf{H}_k^{ij} \right)^T + \mathbf{P}_{k,m}^i \right]^{-1} \\ \hat{\mathbf{x}}_{k|k}^{i,*} &= \hat{\mathbf{x}}_{k|k-1}^i + \mathbf{K}_k^* \left( \mathbf{x}_{k,m}^i - \mathbf{H}_k^{ij} \hat{\mathbf{x}}_{k|k-1}^j \right) \\ \mathbf{P}_{k|k}^{i,*} &= \left( \mathbf{I} - \mathbf{K}_k^* \mathbf{H}_k^{ij} \right) \mathbf{P}_{k|k-1}^i \end{aligned} \tag{6}$$

where  $\hat{\mathbf{x}}_{k|k}^{i,*}$  and  $\mathbf{P}_{k|k}^{i,*}$  are the updated state of the PL<sub>i</sub> and its corresponding covariance without considering the correlation introduced by PL<sub>j</sub>. Then, as in Equation (4), the propagated and updated states can be fused using Equation (2). This fusion can also be performed

during the relative measurement update in a standard KF-based algorithm (Goel et al., 2017):

$$\begin{aligned}
 \mathbf{K}_k &= \mathbf{P}_{k|k-1}^{i,sca} \left( \mathbf{H}_k^{i,j} \right)^T \left[ \mathbf{H}_k^{i,j} \mathbf{P}_{k|k-1}^{i,sca} \left( \mathbf{H}_k^{i,j} \right)^T + \mathbf{P}_{k,m}^{i,sca} \right]^{-1} \\
 \hat{\mathbf{x}}_{k|k}^i &= \hat{\mathbf{x}}_{k|k-1}^i + \mathbf{K}_k \left( \mathbf{x}_{k,m}^i - \mathbf{H}_k^{i,j} \hat{\mathbf{x}}_{k|k-1}^i \right) \\
 \mathbf{P}_{k|k}^i &= \left( \mathbf{I} - \mathbf{K}_k \mathbf{H}_k^{i,j} \right) \mathbf{P}_{k|k-1}^{i,sca}
 \end{aligned} \tag{7}$$

where  $\mathbf{P}_{k|k-1}^{i,sca} = \mathbf{P}_{k|k-1}^i / \omega$  and  $\mathbf{P}_{k,m}^{i,sca} = \mathbf{P}_{k,m}^i / (1 - \omega)$  are two scaled covariances. Another way of performing the fusion during the relative measurement update is given by (Mokhtarzadeh and Gebre-Egziabher, 2014):

$$\begin{aligned}
 \mathbf{P}_{k|k}^i &= \left[ \omega \left( \mathbf{P}_{k|k-1}^i \right)^{-1} + (1 - \omega) \left( \mathbf{H}_k^{i,j} \right)^T \left( \mathbf{P}_{k,m}^i \right)^{-1} \mathbf{H}_k^{i,j} \right]^{-1} \\
 \mathbf{K}_k &= (1 - \omega) \mathbf{P}_{k|k}^i \left( \mathbf{H}_k^{i,j} \right)^T \left( \mathbf{P}_{k,m}^i \right)^{-1} \\
 \hat{\mathbf{x}}_{k|k}^i &= \hat{\mathbf{x}}_{k|k-1}^i + \mathbf{K}_k \left( \mathbf{x}_{k,m}^i - \mathbf{H}_k^{i,j} \hat{\mathbf{x}}_{k|k-1}^i \right)
 \end{aligned} \tag{8}$$

These two ways of accounting for the correlations have less computational cost than the one with fusion performed after the relative measurement update. Since the relative measurement used in this paper is in the form of inter-PL ranges, the correlated covariance components are limited to the states involved in the inter-PL ranges. To incorporate known independent information in the estimates based on the above described algorithms, they need to be modified using the following theory (Li and Nashashibi, 2013):

$$\begin{aligned}
 \mathbf{P}_1 &= \mathbf{P}_{1d} / \omega + \mathbf{P}_{1i} \\
 \mathbf{P}_1 &= \mathbf{P}_{2d} / (1 - \omega) + \mathbf{P}_{2i} \\
 \mathbf{P}^{-1} &= \mathbf{P}_1^{-1} + \mathbf{P}_2^{-1} \\
 \hat{\mathbf{x}} &= \mathbf{P} \left[ \mathbf{P}_1^{-1} \hat{\mathbf{x}}_1 + \mathbf{P}_2^{-1} \hat{\mathbf{x}}_2 \right]
 \end{aligned} \tag{9}$$

where  $\mathbf{P}_{1i}$  and  $\mathbf{P}_{2i}$  are covariance components with known absolute independence and  $\mathbf{P}_{1d}$  and  $\mathbf{P}_{2d}$  are two correlated covariance components. Therefore, to use the SCIF algorithm, the scaled covariances in Equations (7) and (8) have to be added with the independent component before the measurement update. For example, Equation (7) can be changed to:

$$\begin{aligned}
 \mathbf{K}_k &= \mathbf{P}_{k|k-1}^{i,all} \left( \mathbf{H}_k^{i,j} \right)^T \left[ \mathbf{H}_k^{i,j} \mathbf{P}_{k|k-1}^{i,all} \left( \mathbf{H}_k^{i,j} \right)^T + \mathbf{P}_{k,m}^{i,all} \right]^{-1} \\
 \hat{\mathbf{x}}_{k|k}^i &= \hat{\mathbf{x}}_{k|k-1}^i + \mathbf{K}_k \left( \mathbf{x}_{k,m}^i - \mathbf{H}_k^{i,j} \hat{\mathbf{x}}_{k|k-1}^i \right) \\
 \mathbf{P}_{k|k}^i &= \left( \mathbf{I} - \mathbf{K}_k \mathbf{H}_k^{i,j} \right) \mathbf{P}_{k|k-1}^{i,all}
 \end{aligned} \tag{10}$$

where  $\mathbf{P}_{k|k-1}^{i,all} = \mathbf{P}_{k|k-1}^{i,sca} + \mathbf{P}_{k|k-1}^{i,id}$  and  $\mathbf{P}_{k,m}^{i,all} = \mathbf{P}_{k,m}^{i,sca} + \mathbf{P}_{k,m}^{i,id}$  both consist of two covariance components  $\mathbf{P}^{i,sca}$  and  $\mathbf{P}^{i,id}$  representing correlated and independent covariance components, respectively.

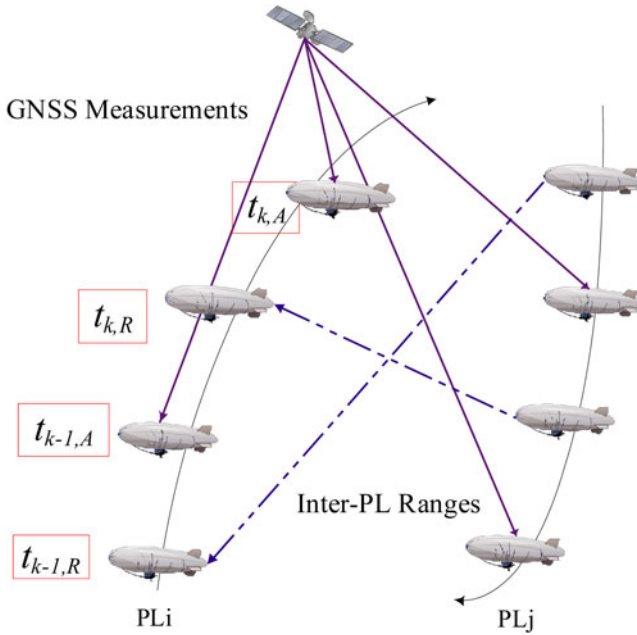


Figure 1. A-PL positioning scheme.

2.2. *GNSS PPP combined with inter-PL range.* GNSS PPP using the dual-frequency Ionosphere-Free (IF) measurement combination is used for the proposed A-PL absolute positioning algorithm. Since these GNSS measurements are independent of the A-PL’s previous state estimates they are processed using standard KF methods.

Figure 1 is a schematic diagram for the A-PL positioning scheme proposed in this paper. PL<sub>i</sub> makes GNSS measurements at time  $t_{k-1,A}$  and  $t_{k,A}$ , and obtains relative measurements from PL<sub>j</sub> at time  $t_{k-1,R}$  and  $t_{k,R}$ . During  $t_{k-1,R}$ ,  $t_{k-1,A}$ ,  $t_{k,R}$  and  $t_{k,A}$ , the state of PL<sub>i</sub> is propagated with its corresponding dynamic model, that is, via the time update. In addition, other sensors such as an INS, barometer or magnetometer can be integrated to enhance the propagated state solution. For simplicity, the estimated parameters in this paper only consider the PL position, velocity, acceleration, and other unknowns that need to be estimated for GNSS PPP. The unknown parameters that need to be estimated are:

$$\mathbf{x}_i = [\mathbf{r}_i \quad \mathbf{v}_i \quad \mathbf{a}_i \quad dt_i \quad Tr_i \quad \mathbf{N}_i] \tag{11}$$

where  $\mathbf{r}_i = [x_i \quad y_i \quad z_i]$  is the PL<sub>i</sub> position,  $\mathbf{v}_i = [v_{x_i} \quad v_{y_i} \quad v_{z_i}]$  is the corresponding velocity,  $\mathbf{a}_i = [a_{x_i} \quad a_{y_i} \quad a_{z_i}]$  is the corresponding acceleration,  $dt_i$  is the PL<sub>i</sub> receiver clock error,  $Tr_i$  is the tropospheric zenith total delay and  $\mathbf{N}_i = [N_i^{s1} \quad N_i^{s2} \quad \dots \quad N_i^{sm}]$  denotes the PL-to-satellite carrier phase ambiguities, which are preserved as “float” values in the estimation process. The velocity and acceleration parameters are used to establish the A-PL dynamic model. The A-PL acceleration parameters are modelled as a first-order Gauss-Markov process, while the other unknown parameters are modelled as random walk processes (Jiang

et al., 2015). The discrete A-PL dynamic model can be expressed as:

$$\begin{cases} \mathbf{r}_{i,k+1} = \mathbf{r}_{i,k} + T \cdot \mathbf{v}_{i,k} + \mathbf{w}_{\mathbf{r}_{i,k}} \\ \mathbf{v}_{i,k+1} = \mathbf{v}_{i,k} + T \cdot \mathbf{a}_{i,k} + \mathbf{w}_{\mathbf{v}_{i,k}} \\ \mathbf{a}_{i,k+1} = \left(1 - \frac{T}{T_c}\right) \mathbf{a}_{i,k} + \mathbf{w}_{\mathbf{a}_{i,k}} \\ dt_{i,k+1} = dt_{i,k} + w_{dt_{i,k}} \\ Tr_{i,k+1} = Tr_{i,k} + w_{Tr_{i,k}} \\ \mathbf{N}_{i,k+1} = \mathbf{N}_{i,k} + \mathbf{w}_{\mathbf{N}_{i,k}} \end{cases} \quad (12)$$

where  $T$  and  $T_c$  are the sampling time and correlation time constant, respectively.  $w_{\cdot,k}$  is the corresponding parameter white noise model. If the A-PL in the network with no GNSS signal access only propagates its positions using the motion Equation (12), the state estimate error drifts due to the noise  $w_{\cdot,k}$  which grows with time without bound. To reduce the error growth, relative measurements between the A-PLs can be used. When the relative measurements are obtained the propagated state of the A-PL can be updated. The relative measurements for the A-PL positioning are the inter-PL ranges:

$$z_{k,R}^{i,j} = \sqrt{(x_i - x_j)^2 + (y_i - y_j)^2 + (z_i - z_j)^2} + n_k^{i,j} \quad (13)$$

where  $[x_j \ y_j \ z_j]$  is the  $PL_j$  position. To perform the relative measurement update for  $PL_i$ ,  $PL_j$  has to share its propagated position and the corresponding covariance  $\hat{\mathbf{x}}_{k|k-1}^j$  and  $\mathbf{P}_{k|k-1}^j$  with  $PL_i$ . Since it may be possible that the bandwidth of data component for the A-PL positioning signal is insufficient to carry all the information, the A-PL could broadcast the data via a separate data link. Therefore,  $PL_i$  has to predict the position of  $PL_j$  at the transmitting time of relative range signal according to the dynamic model in Equation (12). Assuming that the shared trajectory data of  $PL_j$  at time  $t_{k,j}$  is received by  $PL_i$  at  $t_{k,R}$  along with the relative measurement  $z_{k,R}^{i,j}$ , the predicted position for  $PL_j$  is:

$$\mathbf{r}_{t_{k,R}}^j = \mathbf{r}_{t_{k,j}} + t \cdot \mathbf{v}_{t_{k,j}} \quad (14)$$

with  $t = t_{k,R} - t_{k,j}$ . The corresponding covariance  $\mathbf{P}_{k|k-1}^j$  is updated according to Equation (14). If  $PL_i$  and  $PL_j$  are separated by a large distance it is desirable to also take into account the signal travel time, and then  $t$  can be calculated as:

$$t = t_{k,R} - t_{k,j} - z_{k,R}^{i,j} / c \quad (15)$$

where  $c$  is the speed of electromagnetic radiation in a vacuum.

With all the necessary information  $PL_i$  then updates its propagated state using the SCIF algorithm. On the other hand, the GNSS measurements are processed using standard KF methods.

Since each A-PL determines its position in a distributed way, there is no requirement for continuous all-to-all communications, as would be necessary using the centralised approach, to keep track of the cross-correlations between different A-PLs state estimates, even when there is no relative measurement. The A-PL can update its state based on SCIF whenever the inter-PL relative measurement is made. The detailed steps to realise the



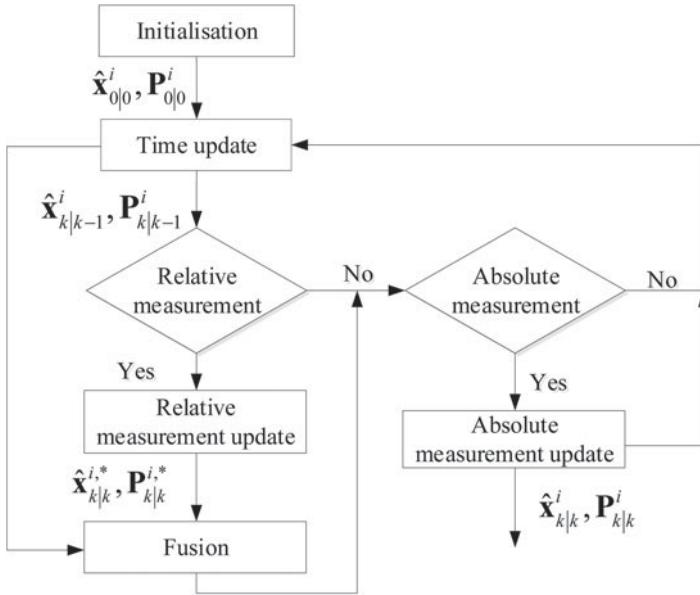


Figure 2. A-PL positioning based on SCIF approach.

distributed localisation algorithm for A-PL positioning are illustrated in Figure 2. In this algorithm two independent updates are involved, one from the relative measurement update and the other from the absolute positioning measurement update. The fusion is performed after the relative measurement update.

3. PREDICTIONS OF ORBIT AND SATELLITE CLOCK CORRECTIONS. Real-time GNSS PPP is dependent on precise and available orbit and satellite clock corrections. An A-PL moving in a GNSS-challenged environment may suffer from disruptions of communication links carrying the required messages. To maintain GNSS PPP positioning performance, the orbit and clock corrections can be predicted using appropriate models when there is a disrupted connection.

3.1. *Real-time orbit and clock corrections.* IGS RTS correction streams are transmitted to users via NTRIP. They are formatted according to the RTCM Services-State Space Representation (RTCM-SSR) message format. The RTS orbit corrections  $\delta\mathbf{O}$  are expressed as radial ( $\delta O_r$ ), along-track ( $\delta O_a$ ) and cross-track ( $\delta O_c$ ) components. Each component has a correction term  $\delta O$  along with its rate-of-change  $\delta\dot{O}$ . The orbit correction at time  $t$  can be calculated as (El-Mowafy et al., 2017):

$$\delta\mathbf{O} = [\delta O_r \quad \delta O_a \quad \delta O_c]^T + [\delta\dot{O}_r \quad \delta\dot{O}_a \quad \delta\dot{O}_c]^T (t - t_0) \tag{16}$$

where  $t_0$  is the reference time included in the RTS message. To apply the corrections to the broadcast orbit  $\mathbf{X}_b$ , the raw RTS corrections have to be transformed to geocentric corrections by using the radial, along-track and cross-track unit vectors ( $e_r, e_a,$  and  $e_c$ ):

$$\mathbf{X}_p = \mathbf{X}_b + [e_r \quad e_a \quad e_c] \delta\mathbf{O} \tag{17}$$

where  $\mathbf{X}_p$  are the precise orbits. The RTS clock correction  $\delta C$  is provided as a correction to the broadcast satellite clock offset. This consists of the correction quantity and its rate-of-change:

$$\delta C = C_0 + C_1 (t - t_0) + C_2 (t - t_0)^2 \quad (18)$$

where  $C_0$ ,  $C_1$  and  $C_2$  are polynomial coefficients. Then, the corrected satellite clock offset  $t_{sat}$  is computed as:

$$t_{sat} = t_b^{sat} + \frac{\delta C}{c} \quad (19)$$

where  $t_b^{sat}$  is the broadcast satellite clock offset.

**3.2. Prediction of orbit and clock corrections.** The availability of the RTS corrections has a significant influence on GNSS PPP positioning. When a correction communication link break occurs, the orbit and satellite clock corrections can be predicted using appropriate models. Since the time series of orbit corrections between each Issue Of Data Ephemeris (IODE) change often exhibit a polynomial pattern, it is possible to represent (and predict) the orbit corrections by using polynomial models (Hadas and Bosy, 2015). For a short period of less than ten minutes, the polynomial models of order two to four with a few minutes of fitting data are able to achieve orbit prediction accuracy of the order of 10 cm. For a period of longer than one hour, it is practical to use the most recent IGU orbit corrections, which are compatible with RTS orbit corrections (El-Mowafy, 2017). However, the IGU clock correction is not good enough to be used as an alternative for the RTS clock correction during RTS outages (Nie et al., 2018). The RTS clock corrections are often predicted as a time series with both polynomial and periodic terms (Heo et al., 2010). The commonly used models for clock prediction are often in the following form (Huang et al., 2014):

$$\delta t = a_0 + a_1 t + a_2 t^2 + \sum_{i=1}^k A_i \sin(\omega_i t + \phi_i) \quad (20)$$

where  $t$  is the time since start of modelling;  $a_0$ ,  $a_1$  and  $a_2$  represent the bias, drift and drift-rate of the clock corrections, respectively;  $k$  is the number of periodic terms and  $A_i$ ,  $\omega_i$  and  $\phi_i$  denote the amplitude, frequency and phase of the corresponding periodic term, respectively.  $a_0$ ,  $a_1$ ,  $a_2$ ,  $A_i$  and  $\phi_i$  are parameters that can be estimated. The quadratic polynomial term can be neglected for current GPS satellites (Nie et al., 2018). Four main sinusoidal periods, including 15 min, 30 min, 3 h and 12 h, are found with fast Fourier transform (FFT) analysis (El-Mowafy et al., 2017). Therefore, Equation (21) can be changed to:

$$\delta t = a_0 + a_1 t + \sum_{i=1}^4 A_i \sin\left(\frac{2\pi}{T_i} t + \phi_i\right) \quad (21)$$

where  $T_i$  is the period. In this paper the scenario of short-term prediction of orbit and clock corrections with fitting data less than 15 min is considered, only one sinusoidal term is used for the clock prediction model. To account for the phase  $\phi_i$  within the sinusoidal term, a

transform can be implemented as follows:

$$\delta t = a_0 + a_1 t + A_s \sin\left(\frac{2\pi}{T_1} t\right) + A_c \cos\left(\frac{2\pi}{T_1} t\right) \quad (22)$$

where  $A_s = A_1 \cos(\phi_1)$  and  $A_c = A_1 \sin(\phi_1)$ . To predict the orbit and clock corrections, the fitting data used for building the prediction models have to be free of outliers. To detect outliers in the orbit fitting data, one simple strategy is to check the differences between the orbit corrections and corresponding values calculated with the polynomial fitting model (El-Mowafy et al., 2017). The outlier can be iteratively detected and removed if the corresponding difference satisfies the following condition:

$$|\Delta\delta O - \mu| > f \cdot \sigma \quad (23)$$

where  $\mu$  and  $\sigma$  represent the average and Standard Deviation (STD) of the orbit difference  $\Delta\delta O$ , respectively, and  $f$  is a scalar threshold, which is recommended to be set to the value of 3 with a 99.7% confidence level. However, this strategy is not suitable for outlier detection of clock correction because the RTS clock correction suffers from abrupt jumps resulting from changes in reference time used by different analysis centres (Chen et al., 2017; El-Mowafy, 2017). To detect the jumps in the clock fitting data, epoch-differenced RTS clock corrections can be used. As with the exclusion condition for orbit corrections, the average and STD of the epoch-differenced RTS clock corrections are calculated. The epoch-differenced RTS clock correction  $\Delta\delta t$  is flagged as an outlier if the absolute deviation around the average is larger than three times the STD. An outlier is detected if the  $\Delta\delta t$  of two consecutive epochs  $t_{n-1}$  and  $t_n$  both satisfy the condition and have opposite signs. Then the clock correction at  $t_{n-1}$  is removed from the clock fitting data. However, if the clock correction at  $t_n$  does not meet the exclusion condition, a jump may exist at  $t_{n-1}$ . To identify the jump, the  $\Delta\delta t$  with an extended period of time from  $t_{n+1}$  to  $t_{n+T}$  needs to be further examined.  $T$  is recommended to be set as 120 s (Chen et al., 2017). If all  $\Delta\delta t$  does not satisfy the exclusion condition, a jump is identified. Then the fitting data for clock prediction model have to be reinitialized from  $t_{n-1}$ .

**4. SEMI-SIMULATION RESULTS AND ANALYSIS.** To validate the A-PL positioning performance based on GNSS PPP, a semi-simulation test was performed on the University of New South Wales (UNSW) campus “Village Green” using a handheld user terminal MagicUT. This device was designed to be used on the Australia-New Zealand Space-Based Augmentation System (SBAS) Testbed. This is a second generation SBAS with Dual Frequency Multi Constellation (DFMC) capability. It is able to perform positioning using a PPP service in real-time. More information can be found at <http://www.ga.gov.au/scientific-topics/positioning-navigation/positioning-for-the-future/satellite-based-augmentation-system>. The A-PL trajectory was simulated by walking, as shown in Figure 3. Raw L1 and L2 dual-frequency GPS measurements were collected for post-processing.

The MagicUT system has several positioning modes: SBAS L1-only, SBAS DFMC, and carrier phase-based PPP. The PPP mode was chosen for the analysis reported here. There are two modes of PPP positioning: ColdStart and QuickStart. The ColdStart needs at least 10 min for the PPP solution to converge to within 40 cm, while the QuickStart uses a precisely surveyed point to ensure almost instantaneous convergence. The QuickStart mode

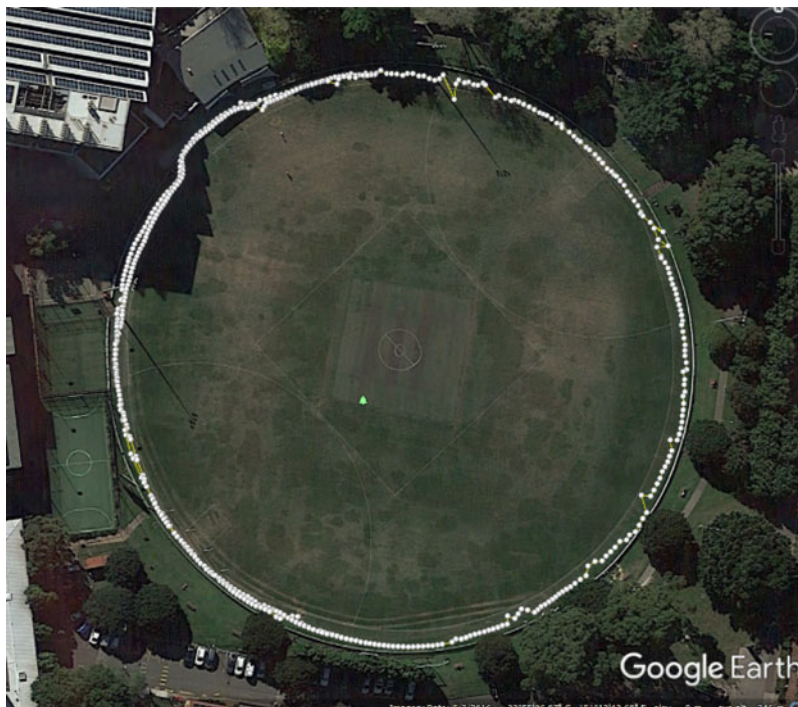


Figure 3. A-PL trajectory for the UNSW test.

was used for the PPP initialisation at a pre-surveyed point. To provide the “ground truth” for the A-PL trajectory, the Piksi Multi, a multi-band multi-constellation RTK GNSS receiver capable of centimetre-level accuracy, was set up alongside the MagicUT so as to use the same antenna, as shown in Figure 4. Approximately 30 min of 1 Hz GPS measurements were collected. The data was post-processed in a float ambiguity PPP solution with real-time IGS combined corrections (IGC), IGC01.

4.1. *Simulation Assumptions.* It is assumed that there were four A-PLs, designated A-PL 1, 2, 3 and 4, moving along predefined paths. The initial positions of the A-PLs were such that they were evenly distributed on a circular trajectory. Each A-PL can measure inter-PL ranges from other A-PLs, as well as make GNSS measurements. For this simulation the data rate of inter-PL ranges was assumed to be 10 Hz. The inter-PL ranges were generated with the “ground truth” provided by the Piksi Multi. The accuracy of the inter-PL range was assumed to be 5 cm and simulated by adding the corresponding magnitude of white noise.

4.2. *A-PL Positioning Performance.* To evaluate the influence of inter-PL ranges on A-PL GNSS PPP positioning, two scenarios for A-PL positioning were simulated. The first scenario was that the A-PL of interest was able to retain the converged GNSS PPP positioning accuracy after the initial setup through the entire mission. Since the experiment was performed on the university campus with some trees impacting the simulated A-PL trajectory, some GNSS signals were intermittently disrupted. To obtain steady converged GNSS PPP positioning accuracy for this scenario, the altitudes provided by the Piksi Multi (with 10 cm accuracy) were used to constrain GNSS PPP positioning accuracy. The second



Figure 4. MagicUT and Piksi Multi hardware setup.

scenario was that A-PL GNSS PPP positioning has to converge to the desired accuracy during the movement. To simulate this scenario, the PPP initialisation with the pre-surveyed point was not used. The A-PL of interest is referred to as A-PL 1 in the following simulation. The influence of the observed A-PL trajectory data on A-PL GNSS PPP positioning with inter-PL ranges was also investigated. As was the case for A-PL 1, the other three A-PLs were simulated with two GNSS PPP positioning scenarios, referred to as scenario 1 and 2. In the simulation, the transmitted trajectory data of the observed A-PLs were assumed to be estimated positions at the previous instant of the received relative measurements. The positions of observed A-PLs were predicted with the state dynamic model before the relative measurement update. A-PL 1 and the other three A-PLs' GNSS PPP positioning performance for the two scenarios are shown in Figure 5. The converged accuracies calculated from 600 s with Root Mean Squared Error (RMSE) are listed in Table 1.

To process the inter-PL range measurements, the SCIF-based distributed positioning algorithms were evaluated and compared with the centralised algorithm. All three forms of SCIF algorithm with the fusion implemented during and after relative measurement update based on Equations (6), (7) and (8) are referred to in the following simulations as SCIF1, SCIF2 and SCIF3, respectively. An EKF was implemented locally on each A-PL to estimate the A-PL positions for the SCIF-based distributed algorithms. The optimum values of  $\omega$  used in the distributed algorithms were determined by minimising the trace of the fused covariance. In addition, the centralised algorithm was operated with the same simulation conditions as the distributed algorithms. This estimates a joint state composed of states of all the A-PLs and tracks the cross-correlations among all the states. The estimated

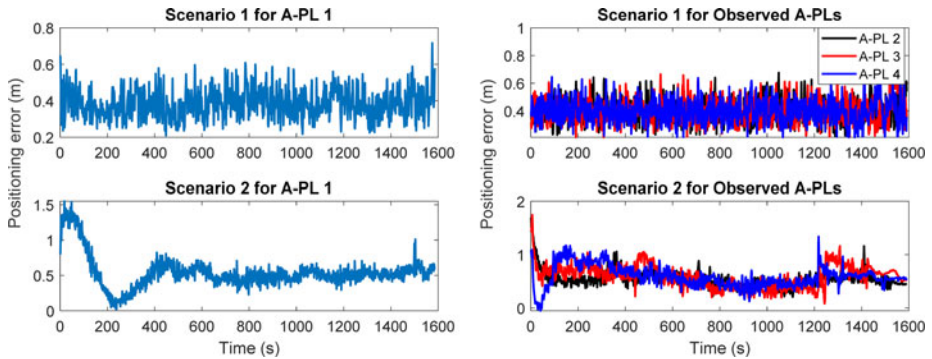


Figure 5. A-PL GNSS PPP positioning results.

Table 1. A-PL GNSS PPP positioning accuracy.

Scenarios	Positioning Errors (m)	
	A-PL 1	Observed A-PLs
1	0.39	0.40
2	0.51	0.55

positioning error and corresponding variances, represented by the diagonal components of matrix  $\mathbf{P}$  calculated during the EKF, for the two positioning scenarios for A-PL 1 with two different observed A-PLs scenarios are shown in Figure 6. The estimated positioning variances in theory reflect the real positioning error. However, it could be affected by the inaccurate predefined covariances of process and measurement noises. Table 2 lists the corresponding converged accuracies and STDs of the estimated positioning errors for all simulated scenarios.

From the positioning performance comparison of scenario 1 for A-PL 1, it can be seen that the A-PL with both GNSS and inter-PL range measurements has almost the same performance in terms of positioning accuracy and smoothness as that for GNSS PPP when the A-PLs with 0.4 m GNSS PPP accuracies are observed. However, when the observed A-PLs' transmitted trajectory data deteriorates, utilising the inter-PL ranges could degrade the A-PL GNSS PPP positioning performance, as can be seen in the right figure of scenario 1 for A-PL 1. Both the centralised and distributed algorithms have to re-converge at the beginning and give slightly worse converged positioning accuracy than in the GNSS PPP-only case. The influence of inter-PL ranges on A-PL GNSS PPP positioning is further demonstrated by the comparison in scenario 2 for A-PL 1. It can be seen that by observing A-PLs with 0.4 m GNSS PPP positioning accuracies the algorithms combining GNSS PPP with inter-PL ranges achieved better converged accuracies than for the GNSS PPP-only case. There is also a tendency for a reduction in GNSS PPP convergence time, as indicated by the positioning results and estimated variances. When the trajectory data of the observed A-PLs degrades, the algorithms with both GNSS and inter-PL range measurements reduce the convergence time of GNSS PPP, except that they converge to worse positioning accuracies. Therefore, to ensure the enhancement of inter-PL ranges in practical applications,

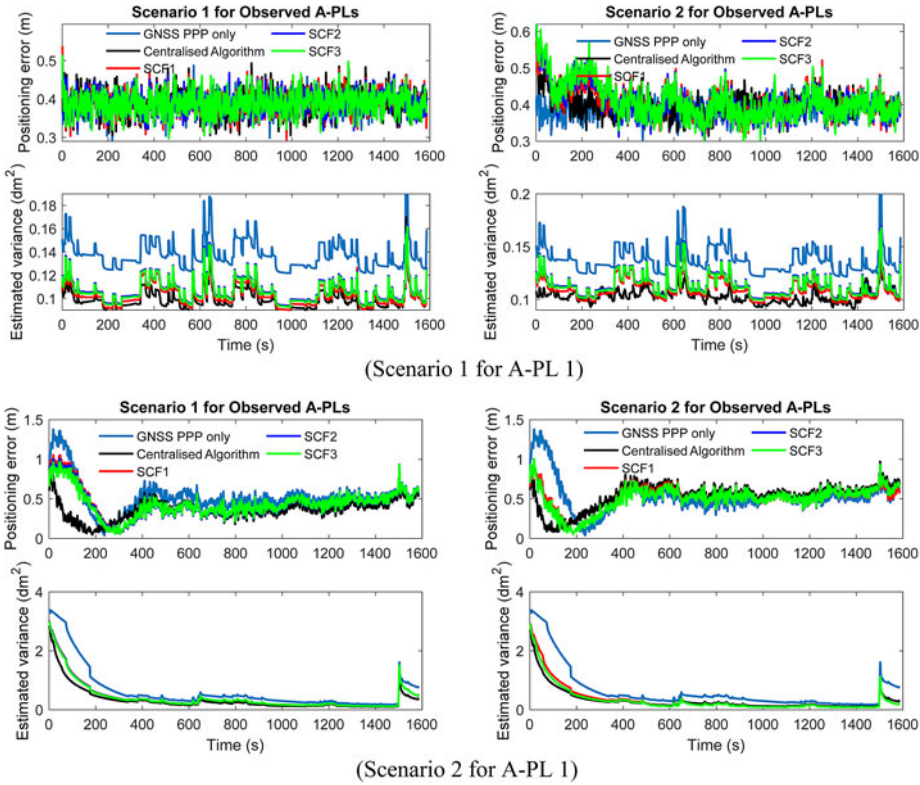


Figure 6. A-PL positioning accuracy of UNSW trial using different algorithms.

Table 2. A-PL positioning accuracy using different algorithms.

Algorithms	Scenario 1 for A-PL 1				Scenario 2 for A-PL 1			
	Observed A-PLs scenario 1		Observed A-PLs scenario 2		Observed A-PLs scenario 1		Observed A-PLs scenario 2	
	RMSE (m)	STD (dm)	RMSE (m)	STD (dm)	RMSE (m)	STD (dm)	RMSE (m)	STD (dm)
GNSS PPP-only	0.39	0.27	0.39	0.25	0.51	0.71	0.51	0.71
Centralised algorithm	0.39	0.28	0.40	0.26	0.40	0.82	0.59	0.72
SCIF1	0.39	0.27	0.40	0.31	0.45	0.92	0.55	0.70
SCIF2	0.39	0.27	0.40	0.30	0.45	0.92	0.55	0.71
SCIF3	0.39	0.27	0.40	0.31	0.45	0.91	0.55	0.71

it is necessary to first check the integrity of the transmitted trajectory data. Interested readers are referred to Goel et al. (2017) for methods of monitoring transmitted information integrity. Furthermore, when more observed A-PLs with good Geometric Dilution Of Precision (GDOP) could be assessed, there will be a reduction in convergence time for GNSS PPP when adding inter-PL range measurements.

Table 3. Mean prediction error of RTS corrections for G17.

Models		Prediction error (cm)	
		Mean	STD
3D orbit	Poly with order 1	10.3	5.9
	Poly with order 2	5.8	4.1
	Poly with order 3	22.8	15.9
Clock	Linear and sinusoidal terms	12.2	7.7
	Only a linear term	13.2	8.8

By comparing the positioning and estimated variance results of the centralised and three SCIF-based distributed algorithms as shown in Figure 6, it can be seen that the centralised algorithm generates a smoother positioning result and has faster convergence due to the precisely tracked cross-correlations among the A-PL states. The left figure of scenario 2 for A-PL 1 illustrates this performance difference. As listed in Table 2, compared with the GNSS PPP-only case, around 20% and 10% improvement in converged positioning accuracy is achieved by the centralised and SCIF-based distributed algorithms, respectively. However, when the observed A-PLs could not provide the trajectory information with satisfactory accuracy as shown in the right figure of scenario 2 for A-PL 1, the converged accuracy of the centralised algorithm is even worse than that of the distributed algorithms. In this case, the distributed algorithms tend to be more robust in dealing with the deteriorated trajectory data of the observed A-PLs. The difference in positioning performance between the centralised and SCIF-based algorithms with scenario 1 for A-PL 1 is much smaller than that with scenario 2 for the A-PL 1. The SCIF-based algorithms can achieve almost the same positioning performance as the centralised algorithm when the GNSS PPP-only is generated by a converged solution. In the case of the three different SCIF-based distributed algorithms, all achieve almost the same positioning performance as shown by all the simulated scenarios. In principle, any one of the three SCIF-based algorithms can be used for A-PL positioning, if the slightly higher computational cost of SCIF1 is not an issue.

4.3. *Analysis of predictions of orbit and satellite clock corrections.* To evaluate the fitting models for short-term RTS correction predictions, the accuracy of IGC predictions with a sliding time window was investigated. The prediction errors were derived from the difference between the predicted values and their known IGC correction values during the prediction period. The periods of the fitting and prediction data were set as 10 min and 30 min, respectively. Three polynomial models with different orders including first, second and third order were investigated. The clock corrections were predicted using the model with linear and sinusoidal terms or only a linear term. For the clock prediction model, the period of the sinusoidal term was first estimated using the FFT. Other parameters involved in the prediction models for the orbit and clock corrections were estimated with a built-in “fitype” function in Matlab.

Table 3 shows one example of the prediction performance for GPS satellite PRN17. The mean and STD prediction errors represent the mean and STD value of all the prediction errors calculated with a sliding window. Since the IGC corrections are not always available, the amount of fitting data in the sliding window may vary, which has to be at least larger than five. The prediction errors only include those calculated before each IODE change or



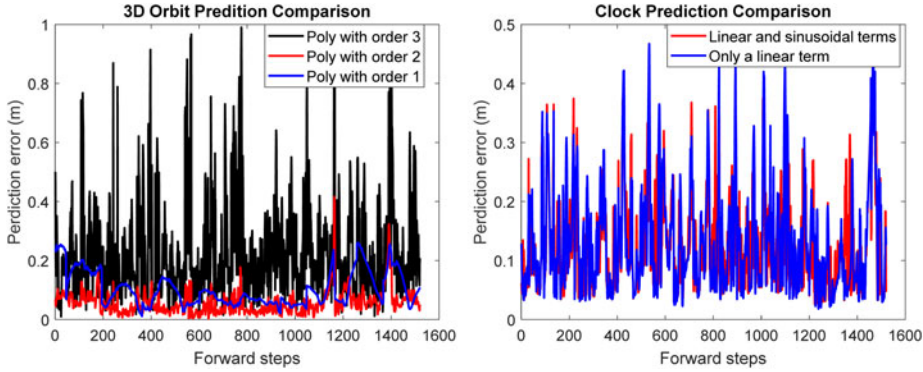


Figure 7. Correction prediction comparison.

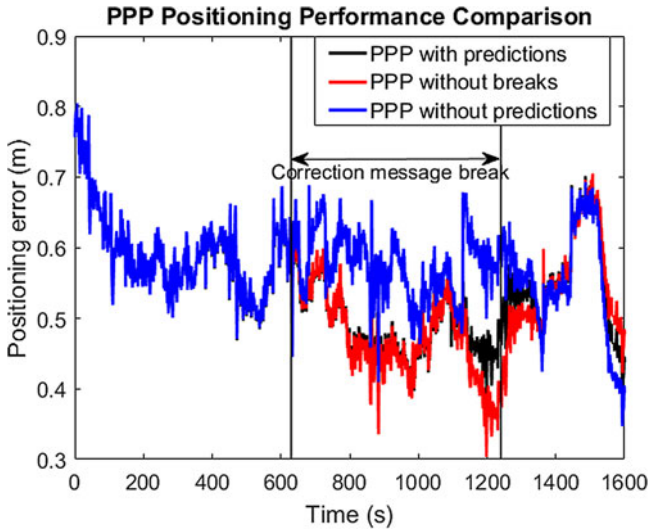


Figure 8. A-PL positioning performance.

Table 4. A-PL positioning accuracy.

Modes	Positioning Errors (m)
PPP with predictions	0.54
PPP without breaks	0.53
PPP without predictions	0.58

clock jump. Figure 7 shows the variation of all prediction errors. It can be seen that the worst model for orbit prediction is the one with order three. The second-order polynomial model achieves the best orbit prediction performance with the minimum mean and STD prediction errors. For satellite clock corrections, the model with linear and sinusoidal terms could obtain slightly better performance than that with only a linear term.

To investigate the effect of correction prediction on A-PL positioning, it was assumed that there was one break in receiving the correction messages added to the A-PL measurements, which lasted around 10 min. The second-order polynomial and linear and sinusoidal models were used for orbit and satellite clock predictions, respectively. The A-PL positioning performance with the correction prediction was compared with the results of PPP positioning without predictions and without breaks, as shown in Figure 8. Table 4 summarises these results. The PPP positioning results obtained with correction predictions are almost the same as those without breaks, which demonstrates the effectiveness of the correction prediction models.

**5. CONCLUDING REMARKS.** In this paper an A-PL positioning concept based on real-time GNSS PPP has been proposed. The inter-PL ranges are used to enhance A-PL positioning. These relative measurements are processed using SCIF algorithms to account for cross-correlations of all A-PL estimated states. SCIF algorithms implemented in three forms were described and investigated. In addition, the short-term prediction of precise orbit and satellite clock corrections with different prediction models was analysed and compared when the correction message communication links was assumed to have been disrupted. Simulations have been performed to study the A-PL positioning performance. The simulation results demonstrate that the A-PL using GNSS PPP combined with inter-PL range measurements is able to achieve better positioning performance in terms of speed of convergence and positioning accuracy than that using the GNSS PPP-only approach. However, the degree of enhancement due to inter-PL ranges is influenced by the transmitted trajectory data of the observed A-PLs, which have to be provided with well-converged accuracy. Although the SCIF-based distributed algorithms indicate limited improvement compared with the centralised algorithm, they are more robust in dealing with degraded transmitted trajectory data of the observed A-PLs. In addition, the second-order polynomial model is preferable for short-term orbit correction predictions compared with the first- or third-order models. The satellite clock corrections can be predicted using either the linear model or one with linear and sinusoidal terms. The prediction models have been shown to be able to effectively reduce the influence of disruption of communication links, and hence to maintain PPP accuracy.

## REFERENCES

- Bisnath, S. and Gao, Y. (2009). *Current state of precise point positioning and future prospects and limitations*. Observing our Changing Earth. International Association of Geodesy Symposia, 133, Springer, Berlin, Heidelberg.
- Carrillo-Arce, L. C., Nerurkar, E. D., Gordillo, J. L. and Roumeliotis, S. I. (2013). Decentralized multi-robot cooperative localization using covariance intersection. In: *2013 IEEE/RSJ International Conference on Intelligent Robots and Systems*, Tokyo, 1412–1417.
- Chandu, B., Pant, R. and Moudgalya, K. (2011). Modeling and simulation of a precision navigation system using pseudolites mounted on airships. *7th AIAA Aviation Technology, Integration and Operations Conference*, Belfast, Northern Ireland.
- Chen, L., Song, W., Yi, W., Shi, C., Lou, Y. and Guo, H. (2017). Research on a method of real-time combination of precise GPS clock corrections. *GPS Solutions*, **21**(1), 187–195.
- de Oliveira, P. S., Morel, L., Fund, F., Legros, R., Monico, J. F. G., Durand, S. and Durand, F. (2017). Modeling tropospheric wet delays with dense and sparse network configurations for PPP-RTK. *GPS Solutions*, **21**(1), 237–250.

- El-Mowafy, A. (2017). Impact of predicting real-time clock corrections during their outages on precise point positioning. *Survey Review*, 2017, 1–10.
- El-Mowafy, A., Deo, M. and Kubo, N. (2017). Maintaining real-time precise point positioning during outages of orbit and clock corrections. *GPS Solutions*, **21**(3), 937–947.
- Gao, Z., Zhang, H., Ge, M., Niu, X., Shen, W., Wickert, J. and Schuh, H. (2017) Tightly coupled integration of multi-GNSS PPP and MEMS inertial measurement unit data. *GPS Solutions*, **21**(2), 377–391.
- García-Crespillo, O., Nossek, E., Winterstein, A., Belabbas, B. and Meurer, M. (2015). Use of High Altitude Platform Systems to augment ground based APNT systems. *2015 IEEE/AIAA 34th Digital Avionics Systems Conference (DASC)*, Prague, Czech Republic, 1–22.
- Geng, J., Meng, X., Dodson, A. H., Ge, M. and Teferle, F. N. (2010) Rapid re-convergences to ambiguity-fixed solutions in precise point positioning. *Journal of Geodesy*, **84**(12), 705–714.
- Goel, S., Kealy, A., Gikas, V., Retscher, G., Toth, C., Brzezinska, D. G. and Lohani, B. (2017). Cooperative localization of unmanned aerial vehicles using GNSS, MEMS Inertial, and UWB sensors. *Journal of Surveying Engineering*, **143**(4), 04017007.
- Gross, J. N., Watson, R. M., D'Urso, S. and Gu, Y. (2016). Flight-test evaluation of kinematic precise point positioning of small UAVs. *International Journal of Aerospace Engineering*, **2016**.
- Hadas, T. and Bosy, J. (2015). IGS RTS precise orbits and clocks verification and quality degradation over time. *GPS Solutions*, **19**(1), 93–105.
- He, C., Yu, B. and Deng, Z. (2016). Wireless time synchronization for multiple UAV-borne pseudolites navigation system. *Proceedings of China Satellite Navigation Conference (CSNC) 2016*, Volume II. Lecture Notes in Electrical Engineering, 389, Springer, Singapore.
- Heo, Y. J., Cho, J. and Heo, M. B. (2010). Improving prediction accuracy of GPS satellite clocks with periodic variation behaviour. *Measurement Science and Technology*, **21**(7), 073001.
- Howard, A., Mataric, M. J. and Sukhatme, G. S. (2002). Mobile sensor network deployment using potential fields: A distributed, scalable solution to the area coverage problem. *Distributed Autonomous Robotic Systems*, **5**, 299–308.
- Huang, G. W., Zhang, Q. and Xu, G. C. (2014). Real-time clock offset prediction with an improved model. *GPS Solutions*, **18**(1), 95–104.
- Jiang, W., Li, Y. and Rizos, C. (2015). Locata-based precise point positioning for kinematic maritime applications. *GPS Solutions*, **19**(1), 117–128.
- Julier, S. J. and Uhlmann, J. K. (1997). A non-divergent estimation algorithm in the presence of unknown correlations. *Proceedings of the 1997 American Control Conference*, Albuquerque, New Mexico, 4, 2369–2373.
- Kia, S. S., Rounds, S. and Martinez, S. (2016). Cooperative localization for mobile agents: a recursive decentralized algorithm based on Kalman-filter decoupling. *IEEE Control Systems*, **36**(2), 86–101.
- Kim, D., Park, B., Lee, S., Cho, A., Kim, J. and Kee, C. (2008). Design of efficient navigation message format for UAV pseudolite navigation system. *IEEE Transactions on Aerospace and Electronic Systems*, **44**(4), 1342–1355.
- Lee, K., Baek, H. and Lim, J. (2016). Enhanced positioning algorithm of ARPS for improving accuracy and expanding service coverage. *Sensors*, **16**(8), 1284.
- Lee, K., Baek, H. and Lim, J. (2017). Relay-based positioning in TDMA networks. *IEEE Systems Journal*. **12**(4), 3849–3852.
- Li, H. and Nashashibi, F. (2013). Cooperative multi-vehicle localization using split covariance intersection filter. *IEEE Intelligent Transportation Systems Magazine*, **5**(2), 33–44.
- Liu, S., Sun, F., Zhang, L., Li, W. and Zhu, X. (2016). Tight integration of ambiguity-fixed PPP and INS: model description and initial results. *GPS Solutions*, **20**(1), 39–49.
- Mokhtarzadeh, H. and Gebre-Egziabher, D. (2014). Cooperative inertial navigation. *Navigation*, **61**(2), 77–94.
- Nie, Z., Gao, Y., Wang, Z., Ji, S. and Yang, H. (2018). An approach to GPS clock prediction for real-time PPP during outages of RTS stream. *GPS Solutions*, **22**(1), 14.
- Small, D. (2017). Method and device for chronologically synchronizing a kinematic location network. U.S. Patent Application 15/327,333.
- Tegedor, J., Øvstedal, O. and Vigen, E. (2014). Precise orbit determination and point positioning using GPS, Glonass, Galileo and BeiDou. *Journal of Geodetic Science*, **4**(1), 65–73.
- Teunissen, P. J. G. and Khodabandeh, A. (2015). Review and principles of PPP-RTK methods. *Journal of Geodesy*, **89**(3), 217–240.

- Tsujii, T., Rizos, C., Wang, J., Dai, L., Roberts, C. and Harigae, M. (2001). A navigation/positioning service based on pseudolites installed on stratospheric airships. *5th Int. Symp. on Satellite Navigation Technology & Applications*, Canberra, Australia.
- Wanasinghe, T. R., Mann, G. K. I. and Gosine, R. G. (2014). Decentralized cooperative localization for heterogeneous multi-robot system using split covariance intersection filter. In: *2014 Canadian Conference on Computer and Robot Vision*, Montreal, QC, Canada, 167–174.
- Wu, Z., Cai, Q. and Fu, M. (2017). Covariance intersection for partially correlated random vectors. *IEEE Transactions on Automatic Control*, **63**(3), 619–629.